Axial Vector Form Factors from Lattice QCD that Satisfy the PCAC Relation

Yong-Chull Jang,[1,*] Rajan Gupta,[2,†] Boram Yoon,[3,‡] and Tanmoy Bhattacharya[2,§]
[1]Brookhaven National Laboratory, Physics Department, Upton, New York 11973, USA
[2]Los Alamos National Laboratory, Theoretical Division T-2, Los Alamos, New Mexico 87545, USA
[3]Los Alamos National Laboratory, Computer Computational and Statistical Sciences, CCS-7, Los Alamos, New Mexico 87545, USA

(Received 20 October 2019; accepted 13 January 2020; published 19 February 2020)

Previous lattice QCD calculations of axial vector and pseudoscalar form factors show significant deviation from the partially conserved axial current (PCAC) relation between them. Since the original correlation functions satisfy PCAC, the observed deviations from the operator identity cast doubt on whether all of the systematics in the extraction of form factors from the correlation functions are under control. We identify the problematic systematic as a missed excited state, whose energy as a function of the momentum transfer squared Q^2 is determined from the analysis of the three-point functions themselves. Its energy is much smaller than those of the excited states previously considered, and including it impacts the extraction of all of the ground state matrix elements. The form factors extracted using these mass and energy gaps satisfy PCAC and another consistency condition, and they validate the pion-pole dominance hypothesis. We also show that the extraction of the axial charge g_A is very sensitive to the value of the mass gaps of the excited states used, and current lattice data do not provide an unambiguous determination of these, unlike the $Q^2 \neq 0$ case. To highlight the differences and improvement between the conventional vs the new analysis strategy, we present a comparison of results obtained on a physical pion mass ensemble at $a \approx 0.0871$ fm. With the new strategy, we find $g_A = 1.30(6)$ and axial charge radius $r_A = 0.74(6)$ fm, both extracted using the z expansion to parametrize the Q^2 behavior of $G_A(Q^2)$, and $g_P^* = 8.06(44)$, obtained using the pion-pole dominance ansatz to fit the Q^2 behavior of the induced pseudoscalar form factor $\tilde{G}_P(Q^2)$. These results are consistent with current phenomenological values.

DOI: 10.1103/PhysRevLett.124.072002

The nucleon axial form factor is an important input needed to calculate the cross section of neutrinos off nuclear targets. It is not well determined experimentally [1]. At present, these form factors are typically extracted from measurements of scattering off nuclear targets and require modeling of nuclear effects [2,3], which introduces uncertainties [4]. Lattice QCD is the best known approach to calculate these from first principles, and in which all systematics can be controlled.

The axial, $G_A(Q^2)$, and the induced pseudoscalar, $\tilde{G}_P(Q^2)$, form factors are extracted from the matrix elements of the isovector axial current $A_\mu \equiv \bar{u}\gamma_5\gamma_\mu d$ between the ground state of the nucleon

$$\langle N^{\boldsymbol{p}}|A_\mu(q)|N^{\boldsymbol{p}'}\rangle = \bar{u}_N^{\boldsymbol{p}}\left(\gamma_\mu G_A + \frac{q_\mu \tilde{G}_P}{2M}\right)\gamma_5 u_N^{\boldsymbol{p}'} \quad (1)$$

and the pseudoscalar form factor $G_P(Q^2)$ from

$$\langle N^{\boldsymbol{p}}|P(q)|N^{\boldsymbol{p}'}\rangle = \bar{u}_N^{\boldsymbol{p}}\gamma_5 G_P u_N^{\boldsymbol{p}'}, \quad (2)$$

where $P = \bar{u}\gamma_5 d$ is the pseudoscalar density, $|N^{\boldsymbol{p}}\rangle$ ($u_N^{\boldsymbol{p}}$) is the nucleon state (spinor) with energy $E_{\boldsymbol{p}}$, mass M, and lattice momentum $\boldsymbol{p} \equiv 2\pi \boldsymbol{n}/La$ with $\boldsymbol{n} \equiv (n_1, n_2, n_3)$. We neglect the induced tensor form factor $\tilde{G}_T$ in Eq. (1) since we assume isospin symmetry, $m_u = m_d$, throughout [5]. All of the form factors will be presented as functions of the spacelike four-momentum transfer $Q^2 \equiv (\boldsymbol{p}')^2 - (E - M)^2 = -q^2; \boldsymbol{p}$ at the sink is fixed to zero.

In our previous work [6], we showed that form factors with good statistical precision can be obtained from lattice simulations; however, these data do not satisfy the partially conserved axial current (PCAC) relation,

$$\frac{\hat{m}}{M}\frac{G_P(Q^2)}{G_A(Q^2)} + \frac{Q^2}{4M^2}\frac{\tilde{G}_P(Q^2)}{G_A(Q^2)} = 1, \quad (3)$$

with the PCAC quark mass $\hat{m}$ defined in Ref. [6]. This failure is also observed in other lattice calculations [7–12]. Since PCAC is an operator relation that is satisfied by the lattice correlation functions, it is important to find and remove the systematics responsible for the deviation at the level of the form factors.

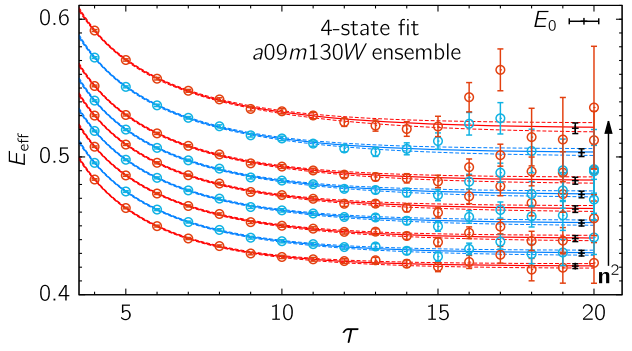

FIG. 1. Data for $E_{\rm eff}(\tau,\boldsymbol{p})$ (circles) and fit results (lines) for $0 \le \boldsymbol{n}^2 \le 6$ and $\boldsymbol{n}^2 = 8$, 10. As $\tau \to \infty$, $E_{\rm eff}(\tau,\boldsymbol{p}) \to E_0(\boldsymbol{p})$.

The central point of this Letter is that the problematic systematic is a missed lower energy excited state. Using a physical pion mass ensemble $a09m130W$ [13,14], we show that the mass and energy gap of this state can be determined from the analysis of nucleon three-point correlation functions. Form factors extracted including these states satisfy PCAC and another consistency condition and constitute a major advance in our understanding of the systematics. Further details of lattice methodology, parameters, statistics, and the interpolating operator used to construct the correlation functions can be found in Refs. [6,13].

The excited-state contamination (ESC) arises because the operator used to create and annihilate the nucleon state couples to the ground and all of the excited and multiparticle states with appropriate quantum numbers. To isolate the ground state matrix elements, we fit the two- and three-point functions $C^{\rm 2pt}_{\boldsymbol{p}}$ and $C^{\rm 3pt}_{\Gamma,\boldsymbol{p}'}$ using their spectral decompositions. The 4-state truncation of $C^{\rm 2pt}_{\boldsymbol{p}}$ is

$$C^{\rm 2pt}_{\boldsymbol{p}}(\tau) = \sum_{i=0}^{3} |\mathcal{A}_i|^2 e^{-E_i^{\rm 2pt}(\boldsymbol{p})\tau}, \tag{4}$$

where $\mathcal{A}_i$ are the amplitudes and $E_i^{\rm 2pt}(\boldsymbol{p})$ the energies for the ith state. The data and fits using Eq. (4) are shown in Fig. 1. There is a reasonable plateau at large τ in $E_{\rm eff}(\tau) \equiv \log\{[C^{\rm 2pt}(\tau)]/[C^{\rm 2pt}(\tau+1)]\}$ for momenta up to $\boldsymbol{n}^2 = 6$. We have checked to see that the lowest E_0 determined from the 4-state fit [13] is consistent with that from a variant of the Prony method [15]. Similarly, the 2-state truncation of $C^{\rm 3pt}_{\Gamma,\boldsymbol{p}'}(t,\tau)$ with Dirac index Γ and operator $O_\Gamma \in A_\mu, P$ is

$$C^{\rm 3pt}_{\Gamma,\boldsymbol{p}'}(t,\tau) = \sum_{i,j=0}^{1} |\mathcal{A}_j||\mathcal{A}'_i|\langle j|O_\Gamma|i'\rangle e^{-E_i t - M_j(\tau-t)}, \tag{5}$$

where $M_0 \equiv M$, $|0\rangle$ and $|n\rangle$ are the ground and nth excited states. The source point is at $t = 0$, the operator is inserted at time t, and the nucleon is annihilated at time τ. The superscript prime denotes that the state could have nonzero momentum $\boldsymbol{p}'$.

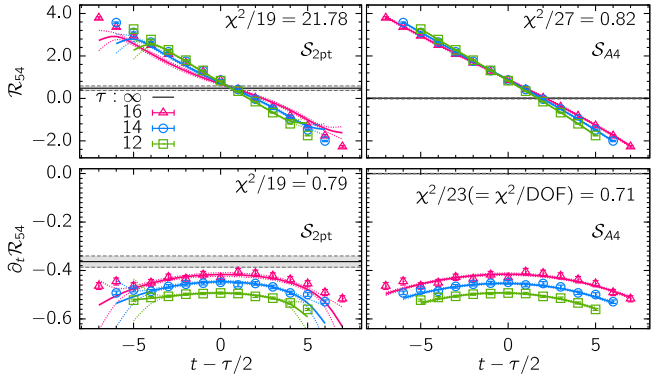

FIG. 2. Data for $\mathcal{R}_{54}$ and $\partial_t \mathcal{R}_{54}$ with $\boldsymbol{p} = (0,0,1)2\pi/La$ and fits to (top panels) A_4 and (bottom panels) $\partial_t A_4$ with the two strategies $\mathcal{S}_{\rm 2pt}$ and $\mathcal{S}_{A4}$. The derivative in $\partial_t \mathcal{R}_{54}$ acts only on $C^{\rm 3pt}_{A4}$ in Eq. (5). The horizontal gray band at approximately zero in the bottom right panel has tiny uncertainty.

To discuss the data, we consider the five ratios $\mathcal{R}$ of the $C^{\rm 3pt}_\Gamma$ to $C^{\rm 2pt}$ functions defined in Ref. [6]:

$$\mathcal{R}_{5i} \to K^{-1}[-q_i q_3 \tilde{G}_P/2M] \quad (i = 1,2), \tag{6}$$

$$\mathcal{R}_{53} \to K^{-1}[-q_3^2 \tilde{G}_P/2M + (M+E_0)G_A], \tag{7}$$

$$\mathcal{R}_{54} \to q_3 K^{-1}[2(M-E_0)\tilde{G}_P + 4MG_A], \tag{8}$$

$$\mathcal{R}_5 \to K^{-1}[q_3 G_P], \qquad K^{-1} \equiv \sqrt{2E_0(E_0+M)}, \tag{9}$$

where "4" is the temporal direction and the spin projection is along "3." As $\tau \to \infty$, these ratios give the ground state matrix elements, whose decomposition into form factors for the nonvanishing momentum combinations is shown in Eqs. (6)–(9). Equivalent momenta are averaged.

For $Q^2 \neq 0$, $\mathcal{R}_{5\mu}$ form an overdetermined system for extracting $\tilde{G}_P$ and G_A, while G_P is uniquely determined from $\mathcal{R}_5$ using Eq. (9). The A_4 correlators have traditionally [6–12] been neglected because fits with E_i and M_i obtained from $C^{\rm 2pt}$ are poor, as shown in Fig. 2 (top left panel). Here, we define two analysis strategies: $\mathcal{S}_{\rm 2pt}$ and $\mathcal{S}_{A_4}$.

$\mathcal{S}_{\rm 2pt}$.—In Eq. (5), we use $M_i = M_i^{\rm 2pt}$ and $E_i = E_i^{\rm 2pt}$, obtained from a 4-state fit to $C^{\rm 2pt}$. With this $\mathcal{S}_{\rm 2pt}$, we have performed up to 3*-state analyses of $C^{\rm 3pt}_\Gamma$ to isolate the ground state matrix elements as discussed in Refs. [6,13]. Form factors obtained using $\mathcal{S}_{\rm 2pt}$ violate PCAC, and correcting for $O(a)$ lattice artifacts in the axial current showed negligible improvement [6]. Furthermore, the violation increases as $Q^2 \to 0$, $a \to 0$, and $M_\pi \to M_\pi^{\rm physical}$.

$\mathcal{S}_{A_4}$.—The ground state's mass and energy are taken from the 4-state fits to $C^{\rm 2pt}$ shown in Fig. 1. For the first excited state, we take $M_1 = M_1^{A4}$ and $E_1 = E_1^{A4}$ from 2-state fits to the A_4 three-point correlator. These are then used in a 2-state analysis of $C^{\rm 3pt}_\Gamma$ with operators A_i and P.

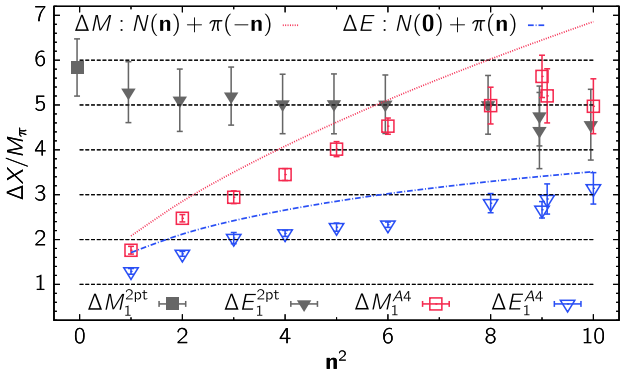

FIG. 3. Energy gaps from $\mathcal{S}_{2pt}$ and $\mathcal{S}_{A_4}$ in units of M_π. The dotted lines show the estimates for noninteracting systems.

Below, we identify the violation of PCAC with $\mathcal{S}_{2pt}$ with a missed lower excited state that can be determined from the analysis of the A_4 correlator, which is very sensitive to the excited state M_i and E_i, as it gets a tiny contribution from the ground state. Its analysis is the basis of the new strategy $\mathcal{S}_{A_4}$, and we highlight two points.

First, fits to the A_4 correlator with $\mathcal{S}_{2pt}$ and $\mathcal{S}_{A4}$ are shown in Fig. 2 (top panels) for $\boldsymbol{n}^2 = 1$. The almost linear (sinh-like) behavior of $\mathcal{R}_{54}$ results from the large ESC (due to the $|0\rangle \leftrightarrow |1\rangle$ transitions) that decreases slowly with τ [16]. The A_4 correlator flips sign at about $\tau/2$, a property under a combined Hermitian conjugate and parity transformation [13]. The χ^2/degrees of freedom (DOF) reduces from 21.8 to 0.8 with $\mathcal{S}_{A_4}$ [17]. The resulting first excited-state mass and energy gaps from $\mathcal{S}_{2pt}$ ($\Delta M_1^{2pt} \equiv M_1^{2pt} - M$, $\Delta E_1^{2pt} \equiv E_1^{2pt} - E_0$) and from $\mathcal{S}_{A_4}$ ($\Delta M_1^{A_4} \equiv M_1^{A_4} - M$, the zero momentum case on the sink side, and $\Delta E_1^{A_4} \equiv E_1^{A_4} - E_0$ with nonzero momentum on the source side) are shown in Fig. 3. It is clear that $\Delta E_1^{A_4}$ and $\Delta M_1^{A_4}$ are much smaller than ΔE_1^{2pt} for $\boldsymbol{n}^2 \lesssim 6$, and they correspond to lower energy excited state(s). By $\boldsymbol{n}^2 \gtrsim 6$, the mass gaps, and therefore the form factors, with the two strategies become similar (see Fig. 4), and the violation of PCAC at larger momentum transfers is smaller as shown in Fig. 5 and in Ref. [6].

Second, the values of $\Delta E_1^{A_4}$ and $\Delta M_1^{A_4}$ and their variation with $\boldsymbol{n}^2$ are consistent with the following picture: the leading contribution of the current $A_4(\boldsymbol{q})$ is to insert or remove a pion with momentum $\boldsymbol{q}$. In that case, $\Delta E_1 = M + E_\pi(\boldsymbol{q}) - E_N(\boldsymbol{q})$ for the $N(\boldsymbol{0})\pi(\boldsymbol{q})$ state, while $\Delta M_1 = E_N(\boldsymbol{q}) + E_\pi(\boldsymbol{q}) - M$ for $N(-\boldsymbol{q})\pi(\boldsymbol{q})$. The impact of such a lower energy $N\pi$ state has been discussed in Refs. [16,21] using effective field theory techniques. These ΔE_1 and ΔM_1, for noninteracting lattice states and using the relativistic dispersion relation that our data support, are shown with dotted lines in Fig. 3.

It is very important to note that, in such 2-state fits, the contributions of all possible excited states are, in practice, lumped into one. Future higher statistics calculations are needed to resolve and include more states.

Applying the strategy $\mathcal{S}_{A4}$ to the three spatial correlators A_i and the P correlator gives very different values for the ground state matrix elements, and thus the form factors, especially for $\boldsymbol{n}^2 \lesssim 5$. On the other hand, the χ^2/DOF of the fits with full covariance matrix are similar. The same is true of fits to $\mathcal{C}^{2pt}$, in which the number of points sensitive to ESC are small. Thus, the two strategies, with very different ΔE and ΔM, are not distinguished based on χ^2/DOF with current statistics (165×10^3 measurements on 1290 configurations) [13]. (The data and fits to $\mathcal{C}^{2pt}$, A_i, and P comparing $\mathcal{S}_{A_4}$ and $\mathcal{S}_{2pt}$ are shown in the Supplemental Material [17]). In $\mathcal{C}^{3pt}_{A_i}$, the variation of ESC over a limited range of τ ($10 \le \tau \le 16$ in our case) is essentially linear and similar, whereas the $\tau \to \infty$ limit, i.e., the value of the ground state matrix element, depends strongly on them. In short, it is very important to determine ΔE and ΔM reliably first since the χ^2/DOF of the fits to the A_i do not provide a good metric for differentiation.

The results for the three form factors G_A, $\tilde{G}_P$, and G_P are compared in Fig. 4. The effect of using $\mathcal{S}_{A4}$ is clear and largest for $\boldsymbol{n}^2 = 1$. In particular, the change in $G_A(Q^2)$ is apparent only for $\boldsymbol{n}^2 = 1$; consequently, data at smaller Q^2 are needed to quantify its $Q^2 \to 0$ limit, i.e., the charge g_A. The pattern, that the effect increases as $Q^2 \to 0$, $a \to 0$, and $M_\pi \to M_\pi^{\text{physical}}$, is confirmed by the analysis of the 11

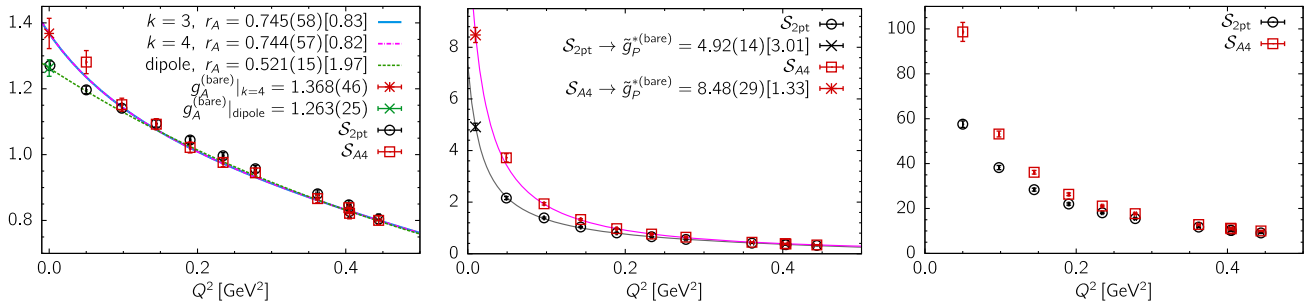

FIG. 4. Comparison of (left panel) G_A, (middle panel) $\tilde{G}_P \times (m_\mu/2M)$, and (right panel) G_P obtained using the two strategies $\mathcal{S}_{A4}$ and $\mathcal{S}_{2pt}$. The lines show the dipole and z^k-expansion fits to G_A from $\mathcal{S}_{A4}$ and the PPD ansatz to $\tilde{G}_P$.

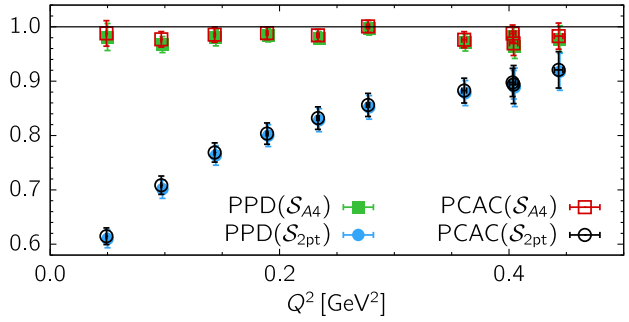

FIG. 5. Tests of the PCAC relation, Eq. (3), and the PPD hypothesis, Eq. (10), with the two strategies $\mathcal{S}_{A4}$ and $\mathcal{S}_{2pt}$.

ensembles described in Ref. [13] and partly presented in Ref. [22].

With G_A, $\tilde{G}_P$, and G_P in hand, we test the PCAC relation, Eq. (3), and the pion-pole dominance (PPD) hypothesis, which relates $\tilde{G}_P$ to G_A as

$$\frac{\tilde{G}_P(Q^2)}{G_A(Q^2)}\frac{Q^2+M_\pi^2}{4M^2}=1, \tag{10}$$

in Fig. 5. Both relations are satisfied to within 5% at all Q^2 with $\mathcal{S}_{A4}$, whereas the deviation grows to about 40% with $\mathcal{S}_{2pt}$ at $\boldsymbol{n}^2=1$, as first pointed out in Ref. [6]. What is also remarkable is that the PPD relation with the proportionality factor $4M^2$ provided by the Goldberger-Treiman relation [23] tracks the improvement in PCAC. In fact, the data for the two tests overlap at all Q^2.

The next test, shown in Fig. 2 (bottom panels), demonstrates that the relation $\partial_t A_4=(M-E)A_4$ is satisfied by the ground state matrix elements only for $\mathcal{S}_{A4}$. The values of $(M-E)A_4$ are essentially zero in both cases for $\mathcal{S}_{2pt}$ because $(M-E)$ is small.

The axial charge g_A is obtained from the A_3 correlator with $\boldsymbol{q}=0$, as shown in Eq. (7). The relevant ΔM is typically taken from the two-point fit and cannot be extracted from A_4. Candidates for the lowest energy excited state with spin-isospin-parity $\frac{1}{2}(\frac{1}{2}^+)$ at $\boldsymbol{q}=0$ are $N\pi\pi$ and $N(\boldsymbol{p})\pi(-\boldsymbol{p})$. Both are lighter than the radial excitations N(1440) and N(1710) and dominate their decay. Their relativistic noninteracting energies, in a box of size $L/a=64$ used for the $a09m130W$ ensemble, are about 1230 MeV ($a\Delta M_1\approx 0.12$). In our analysis, the only quantity that enters is the mass gap, not the specifics of the excited state, so we take the common value, $a\Delta M_1=0.12(4)$ for the prior, in the reanalysis of A_3 to extract g_A. These fits give g_A within the range 1.29–1.31 depending on the value of τ used in the fit compared to $g_A=1.25(2)$ using the $\mathcal{S}_{2pt}$ value given in Ref. [18]. Unfortunately, fits with priors in the range $0.1\lesssim a\Delta M_1\lesssim 0.4$ are not distinguished on the basis of χ^2/DOF. The output ΔM_1 tracks the input prior, and the value of g_A increases as the prior value is decreased. This implies a large systematic uncertainty in g_A unless the relevant ΔM_i are known *a priori* and input into the fit. An estimate of ΔM_1 is $\Delta M_1^{A4}(\boldsymbol{n}^2=1)\approx 1.8M_\pi$, which roughly corresponds to the $N(-\boldsymbol{p})\pi(\boldsymbol{p})$ state mentioned above. Using this ΔM_1^{A4} in a 2-state fit to $A_3(\boldsymbol{0})$ gives $g_A=1.30(6)$, with the axial current renormalization factor, $Z_A=0.95(4)$, taken from Ref. [18].

Parenthetically, fits to extract the scalar and tensor charges g_S and g_T with priors over the same range are much more stable: the value of the output ΔM_1 is far less sensitive to the prior, and the results vary by $\lesssim 2\sigma$. This analysis will be presented in a separate publication.

Note that with infinite statistics one can extract all of the relevant excited states from the nucleon two-point function. With finite statistics, a known methodology is to construct a large basis of interpolating operators, including operators overlapping primarily with multiparticle states, and solve the generalized eigenvalue problem [24] in a variational approach [25–29]. In either case, $\mathcal{S}_{2pt}$ should become a viable strategy. The latter option will be explored in future calculations.

The second way that we extract g_A is to parametrize the Q^2 dependence of $G_A(Q^2\neq 0)$ using the z expansion and the dipole ansatz. The z^k-expansion fits, using the process defined in Refs. [6,13], give $g_A=1.30(7)$ for $\mathcal{S}_{A4}$ compared to $g_A=1.19(5)$ using $\mathcal{S}_{2pt}$. These results are stable for $k\geq 3$. The dipole fit gives $g_A=1.20(6)$ with a large χ^2/DOF $=1.97$, and the results are essentially the same for $\mathcal{S}_{A4}$ and $\mathcal{S}_{2pt}$ and miss the point at low Q^2, as can be seen in Fig. 4 (left panel). One can fix the dipole fit by putting a cut on Q^2; however, in this Letter, we choose to neglect it.

The root-mean-squared charge radius, extracted using the same z-expansion fits, is $r_A=0.74(6)$ fm with $\mathcal{S}_{A4}$ and $r_A=0.45(7)$ fm with $\mathcal{S}_{2pt}$. For comparison, (i) a weighted world average of (quasi)elastic neutrino and antineutrino scattering data is 0.666(17) fm [1], (ii) charged pion electroproduction experiments give 0.639(10) fm [1], and (iii) a reanalysis of the deuterium target data gave 0.68(16) fm [30].

The induced pseudoscalar charge g_P^*, defined as $g_P^*\equiv(m_\mu/2M)\times\tilde{G}_P(0.88m_\mu^2)$, is obtained by fitting $\tilde{G}_P(Q^2)$ using the small Q^2 expansion of the PPD ansatz:

$$\frac{m_\mu}{2M}\tilde{G}_P(Q^2)=\frac{c_1}{M_\pi^2+Q^2}+c_2+c_3Q^2. \tag{11}$$

We obtain $g_P^*=8.06(44)$ with $\mathcal{S}_{A4}$ and $g_P^*=4.67(24)$ with $\mathcal{S}_{2pt}$, while the MuCap experiment gave $g_P^*=8.06(55)$ [31,32]. We caution the reader that all results summarized in Table I are at fixed lattice spacing a. Extrapolation to $a\to 0$ is needed before making a comparison to the experimental values, compiled here for completeness.

An attempt to resolve the PCAC conundrum was presented in Ref. [33] using the projected currents $A_\mu^\perp\equiv[g_{\mu\nu}-(\bar{p}_\mu\bar{p}_\nu/\bar{p}^2)]A_\nu$ and $P^\perp\equiv P-(1/2i\hat{m})(\bar{p}_\mu\bar{p}_\nu/\bar{p}^2)\partial_\mu A_\nu$.

TABLE I. Results for $a09m130W$ from both strategies, $\mathcal{S}_{A4}$ and $\mathcal{S}_{2pt}$. g_A is obtained in three ways, as discussed in the text, and r_A and g_P^* are obtained from z^4 fits.

	$g_A\|_{3pt}$	$g_A\|_{z^4-exp}$	$g_A\|_{dip}$	r_A (fm)	g_P^*
$\mathcal{S}_{A4}$	1.30(6)	1.30(7)	1.20(6)	0.74(6)	8.06(44)
$\mathcal{S}_{2pt}$	1.25(2)	1.19(5)	1.20(5)	0.45(7)	4.67(24)

We contend that these do not resolve the lower energy state and do not solve the problem. The currents $A_\mu^\perp$ and $P^\perp$ are a rotation in the basis of the five currents A_μ and P. The $A_i^\perp$ currents essentially remain within the space of the A_i currents; thus, $\mathcal{S}_{2pt}$ strategy with $A_i^\perp$ gives G_A and $\tilde{G}_P$ values that are essentially unchanged, and one continues to get a low value for g_P^* [33]. The operator $A_4^\perp$ is mostly rotated into the A_i and no longer shows a large ESC. Their "fix" to PCAC comes from $P^\perp$, which gets its dominant contribution from $\partial_t A_4$. Our analysis of the $a09m130W$ ensemble shows that this contribution is roughly 3 times that of P due to the small value of the PCAC mass $\hat{m}$ in the definition $P^\perp$. Note that, by construction, the total contribution of $(P^\perp - P)$ is supposed to be zero in the ground state, whereas the value of the bare $G_P(\boldsymbol{n}^2 = 1)$ changes from 58(1) using P to 175(8) using $P^\perp$. Using the same raw data for P but with strategy $\mathcal{S}_{A4}$, we instead get $G_P(\boldsymbol{n}^2 = 1) = 99(4)$, and PCAC is fixed because all three ground state matrix elements, and thus G_A, $\tilde{G}_P$, and G_P, change upon including the lower energy excited state.

Conclusions.—All previous lattice calculations of the three form factors G_A, $\tilde{G}_P$, and G_P showed significant violations of the PCAC relation, Eq. (3) [6–12]. This failure had cast doubts on the lattice methodology for extracting nucleon form factors. In this Letter, we show that the systematic responsible for the violation is lower energy excited states missed in previous analyses. Furthermore, we show how to estimate the energy of this lower state from fits to the A_4 three-point function. Detailed analysis of the A_4 correlator had previously been neglected, as it is dominated by ESC and is not needed to extract the form factors. With this lower excited state, lattice data satisfy PCAC to within 5%, the level expected with current statistical and systematic errors. Also, the identity $\partial_t A_4 = (M - E)A_4$ holds for the ground state matrix elements, and pion-pole dominance works.

We demonstrate the improvement in G_A, $\tilde{G}_P$, and G_P by analyzing a physical mass ensemble with $a \approx 0.0871$ fm, $M_\pi \approx 138$ MeV [6,13]. Parametrizing the Q^2 behavior of $G_A(Q^2)$ using the z expansion, we extract the axial charge radius $r_A = 0.74(6)$ fm and the axial charge $g_A = 1.30(7)$. The dipole ansatz does not fit the data well, and results from it are dropped. We fit $\tilde{G}_P(Q^2)$ using the PPD ansatz and find $g_P^* = 8.06(44)$. To obtain results in the continuum limit, analysis of the 11 ensembles described in Ref. [13] is in progress.

The extraction of g_A from the A_3 correlator at zero momentum is also sensitive to the input value of the mass gap ΔM_1. Since this ΔM_1 cannot be extracted from the A_4 correlator, as it vanishes at zero momentum, further work is required to identify the dominant excited states contaminating the extraction of g_A. The bottom line is, the resolution of excited states is important for all calculations of nucleon matrix elements, in particular of the axial current, as shown here.

We thank the MILC Collaboration for providing the $2 + 1 + 1$-flavor highly improved staggered quark lattices. The calculations used the CHROMA software suite [34]. Simulations were carried out on computer facilities at (i) the National Energy Research Scientific Computing Center, a U.S. DOE Office of Science User Facility supported by the Office of Science of the U.S. Department of Energy under Contract No. DE-AC02-05CH11231; (ii) the Oak Ridge Leadership Computing Facility at the Oak Ridge National Laboratory, which is supported by the Office of Science of the U.S. Department of Energy under Contract No. DE-AC05-00OR22725; (iii) the USQCD Collaboration, which is funded by the Office of Science of the U.S. Department of Energy; and (iv) Institutional Computing at Los Alamos National Laboratory. T. B. and R. G. were partly supported by the U.S. Department of Energy, Office of Science, Office of High Energy Physics, under Contract No. DE-AC52-06NA25396. T. B., R. G., Y.-C. J., and B. Y. were partly supported by the LANL LDRD program. Y.-C. J. is partly supported by U.S. Department of Energy under Contract No. DE-SC0012704.

*ypj@bnl.gov
†rajan@lanl.gov
‡boram@lanl.gov
§tanmoy@lanl.gov

[1] V. Bernard, L. Elouadrhiri, and U.-G. Meissner, J. Phys. G **28**, R1 (2002).
[2] J. Carlson, S. Gandolfi, F. Pederiva, S. C. Pieper, R. Schiavilla, K. E. Schmidt, and R. B. Wiringa, Rev. Mod. Phys. **87**, 1067 (2015).
[3] A. A. Aguilar-Arevalo *et al.* (MiniBooNE Collaboration), Phys. Rev. D **81**, 092005 (2010).
[4] R. J. Hill, P. Kammel, W. J. Marciano, and A. Sirlin, Rep. Prog. Phys. **81**, 096301 (2018).
[5] T. Bhattacharya, V. Cirigliano, S. D. Cohen, A. Filipuzzi, M. González-Alonso, M. L. Graesser, R. Gupta, and H.-L. Lin, Phys. Rev. D **85**, 054512 (2012).
[6] R. Gupta, Y.-C. Jang, H.-W. Lin, B. Yoon, and T. Bhattacharya, Phys. Rev. D **96**, 114503 (2017).
[7] G. S. Bali, S. Collins, B. Glässle, M. Göckeler, J. Najjar, R. H. Rödl, A. Schäfer, R. W. Schiel, W. Söldner, and A. Sternbeck, Phys. Rev. D **91**, 054501 (2015).
[8] J. Green, N. Hasan, S. Meinel, M. Engelhardt, S. Krieg, J. Laeuchli, J. Negele, K. Orginos, A. Pochinsky, and S. Syritsyn, Phys. Rev. D **95**, 114502 (2017).

[9] C. Alexandrou, M. Constantinou, K. Hadjiyiannakou, K. Jansen, C. Kallidonis, G. Koutsou, and A. Vaquero Aviles-Casco, Phys. Rev. D **96**, 054507 (2017).
[10] S. Capitani, M. Della Morte, D. Djukanovic, G. M. von Hippel, J. Hua, B. Jäger, P. M. Junnarkar, H. B. Meyer, T. D. Rae, and H. Wittig, Int. J. Mod. Phys. A **34**, 1950009 (2019).
[11] K.-I. Ishikawa, Y. Kuramashi, S. Sasaki, N. Tsukamoto, A. Ukawa, and T. Yamazaki (PACS Collaboration), Phys. Rev. D **98**, 074510 (2018).
[12] E. Shintani, K.-I. Ishikawa, Y. Kuramashi, S. Sasaki, and T. Yamazaki, Phys. Rev. D **99**, 014510 (2019).
[13] Y.-C. Jang, R. Gupta, H.-W. Lin, B. Yoon, and T. Bhattacharya, Phys. Rev. D **101**, 014507 (2020).
[14] A. Bazavov *et al.* (MILC Collaboration), Phys. Rev. D **87**, 054505 (2013).
[15] G. T. Fleming, S. D. Cohen, H.-W. Lin, and V. Pereyra, Phys. Rev. D **80**, 074506 (2009).
[16] O. Bar, Phys. Rev. D **99**, 054506 (2019).
[17] See Supplemental Material at http://link.aps.org/supplemental/10.1103/PhysRevLett.124.072002, which includes Refs. [13,18–20], for fit qualities and parameters for all momenta.
[18] R. Gupta, Y.-C. Jang, B. Yoon, H.-W. Lin, V. Cirigliano, and T. Bhattacharya, Phys. Rev. D **98**, 034503 (2018).
[19] B. Yoon *et al.*, Phys. Rev. D **95**, 074508 (2017).
[20] Y.-C. Jang, T. Bhattacharya, R. Gupta, H.-W. Lin, and B. Yoon (PNDME Collaboration), Proc. Sci. LATTICE2018 (**2018**) 123 [arXiv:1901.00060].
[21] M. T. Hansen and H. B. Meyer, Nucl. Phys. **B923**, 558 (2017).
[22] Y.-C. Jang, R. Gupta, T. Bhattacharya, H.-W. Lin, and B. Yoon (PNDME Collaboration), Proc. Sci. LATTICE2019 (**2019**) 131 [arXiv:2001.11592].
[23] M. L. Goldberger and S. B. Treiman, Phys. Rev. **111**, 354 (1958).
[24] G. Fox, R. Gupta, O. Martin, and S. Otto, Nucl. Phys. **B205**, 188 (1982).
[25] R. G. Edwards, J. J. Dudek, D. G. Richards, and S. J. Wallace, Phys. Rev. D **84**, 074508 (2011).
[26] C. Alexandrou, T. Korzec, G. Koutsou, and T. Leontiou, Phys. Rev. D **89**, 034502 (2014).
[27] C. B. Lang and V. Verduci, Int. J. Mod. Phys. Conf. Ser. **26**, 1460056 (2014).
[28] J. J. Dudek, in Proceedings of the 13th Conference on the Intersections of Particle and Nuclear Physics (CIPANP 2018), Palm Springs, CA, 2018 (2018) [arXiv:1809.07350].
[29] R. A. Briceno, J. J. Dudek, and R. D. Young, Rev. Mod. Phys. **90**, 025001 (2018).
[30] A. S. Meyer, M. Betancourt, R. Gran, and R. J. Hill, Phys. Rev. D **93**, 113015 (2016).
[31] V. A. Andreev *et al.* (MuCap Collaboration), Phys. Rev. Lett. **110**, 012504 (2013).
[32] V. A. Andreev *et al.* (MuCap Collaboration), Phys. Rev. C **91**, 055502 (2015).
[33] G. S. Bali, S. Collins, M. Gruber, A. Schäfer, P. Wein, and T. Wurm, Phys. Lett. B **789**, 666 (2019).
[34] R. G. Edwards and B. Joo (SciDAC, LHPC, and UKQCD Collaborations), Nucl. Phys. B, Proc. Suppl. **140**, 832 (2005).